In presenting this dissertation/thesis as a partial fulfillment of the requirements for an advanced degree from Emory University, I agree that the Library of the University shall make it available for inspection and circulation in accordance with its regulations, governing materials of this type. I agree that permission to copy form, or to publish, this thesis/dissertation may be granted by the professor under whose direction it was written, or, in his/her absence, by the Dean of the Graduate School when such copying or publication is solely for scholarly purposes and does not involve potential financial gain. It is understood that any copying from, or publication of, this thesis/dissertation which involves potential financial gain will not be allowed without written permission.

_____

Kornelius D. Bankston

Encapsulation of Small Molecules with Nanotubes

By

Kornelius D. Bankston

Master of Science

Department of Chemistry

David G. Lynn, Ph.D.
Adviser

CoraMacBeth, Ph.D.
Committee Member

Stefan Lutz, Ph.D.
Committee Member

Accepted:

Lisa A.Tedesco, Ph.D.
Dean of the Graduate School

Date

Encapsulation of Small Molecules in Peptide Nanotubes

By

Kornelius D. Bankston

B.S., Morehouse College, Department of Chemistry, 2003

Adviser: David G. Lynn, Ph.D.

An Abstract of

A thesis submitted to the Faculty of the Graduate

School of Emory University in partial fulfillment

of the requirements for the degree of

Master of Science

Department of Chemistry

2007

The discovery of the peptide nanotube has given great optimism to the area of gene delivery systems. These structures are unique in that they were discovered from a truncated segment of Aβ(1-42). This fragment has been reported as being a critical sequence in the formation of amyloid plaques of Alzheimer's disease . The novelty of these peptide nanotubes, besides their ability to self assembly into homogeneous tubular structures, includes the self assembly of nucleobase peptide nanotubes with high specificity and localized functionality. Preliminary evidence suggests that the cytosines in the nucleobase peptide nanotube are on the surface of the single layer nanotube . The investigation of the location of the nucleobases is important in ascertaining the structure of the nucleobase peptide nanotube. To further the knowledge and versatility of this peptide sequence I discovered that small molecules interact with the nucleobase peptide nanotube.

Encapsulation of Small Molecules in Peptide Nanotubes

By

Kornelius D. Bankston

B.S., Morehouse College, Department of Chemistry, 2003

Adviser: David G. Lynn, Ph.D.

A thesis submitted to the Faculty of the Graduate
School of Emory University in partial fulfillment
of the requirements for the degree of
Master of Science

Department of Chemistry

2007

TABLE OF CONTENTS

ACKNOWLEDGEMENTS

I am extremely grateful to have had the opportunity to be a part of this University and Chemistry Department. I have gained a lot of insight about my potential and the love I have for higher learning. It is with the advisement of Dr. David Lynn that I came to Emory University. I am thankful for his support! My committee members Drs. Cora MacBeth and Stefan Lutz your help in this process has developed me into a more critical thinker. Thank you!

It is with the help of Dr. Anil Mehta that I was able to think through the Science to get this work completed. He has proven to be a great Teacher and Scientist without his help I would have been lost. Thank You! Dr. Kun Lu, Dr. Jijun Dong, and Peng Liu I am happy that you took the time to help me. I wish much success in all your endeavors. Thank you! The Lynn Lab are some troopers and very hard workers, your help has been priceless. Rong Ni, Yan Liang, Seth Childers, James Simmons, Yi Xu, Andrew Palmer, Dr. Trey Maddox and all the current and past members are some talented young scientist. Thank you for allowing me to be a part of the lab family.

To my crew, Kim Becnel Davis and Dr. Rhonda L. Moore, where would I be if I didn't have your encouraging words and our weekly arguments? I am thankful that God saw fit for me to have two women around me daily, who really had my back. Thank you! To the Emory University NOBCChE members you all have been diligent in keeping the chapter alive and together. Thank you!

To God, my mom and my family who have been the foundation in my life. I am thankful that you believe in me and my abilities. Thank you for not allowing me to give up on myself.

Our deepest fear is not that we are inadequate. Our deepest fear is that we are powerful beyond measure. It is our light, not our darkness that most frightens us. We ask ourselves, Who am I to be brilliant, gorgeous, talented, fabulous? Actually, who are you *not* to be? You are a child of God. Your playing small does not serve the world. There is nothing enlightened about shrinking so that other people won't feel insecure around you. We are all meant to shine, as children do. We were born to make manifest the glory of God that is within us. It is not just in some of us; it is in everyone. And as we let our own light shine, we unconsciously give other people permission to do the same. As we are liberated from our own fear, our presence automatically liberates others.

By: Marianne Williamson

List of Figures

LIST OF TABLES

Introduction

Nanomaterials

The projected impact of nanotechnology has been touted as a second industrial revolution. Not third, fourth, or fifth, because despite similar predictions for technologies such as computers and robotics, nothing has as yet eclipsed the first. The original industrial revolution transformed our way of life. At the level of the individual it doubled average lifespan; at the level of national affairs it made possible truly global civilizations. Will nanotechnology measure up on that scale? Reaching a solid understanding of new technology-the understanding necessary to judge its effects is an intellectual adventure. (K..Eric Drexler, ,Los Altos, California,August 2004, NanoFuture)

Nanotechnology involves measuring, designing, and manipulating material at the atomic, molecular, and supramolecular levels [1]. The field seeks to understand and develop materials, structures, devices, and systems (spanning form 1 to 100nm in length) [1]. Advancements have been made in understanding how nanomaterials self- organize, self- repair, and self- replicate [2].

Nanomaterials are being used in an array of applications i.e. Biomedical Nanotechnology, implants, diagnostics and screening. Nanobiomedicine takes advantage of the nanoscale principles to build new materials and biosystems [1]. Technological advances have been made in drug synthesis, brain understanding, body part replacement, visualization, and instruments for medical interventions [1]. Nanotechnology is advancing in understanding the manipulation of single nanostructure to nanosystems.

For example, carbon nanotubes are formed through self organization of carbon atoms. Nanotube assembly requires reactive carbon atoms at high temperatures [3]. Carbon atoms then organize in regular patterns on the surface of metal particles resulting in long chains of assembled carbon atoms [3].

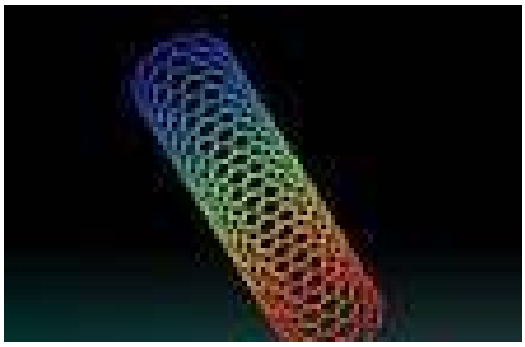

Figure 1.1 Cartoon of a carbon nanotube [1].

Self-organization results in non-equilibrium products (**Figure 1.2**) [1]. In this method the structures are assembled all at once. It is through a high degree non equilibrium that carbon atom organize, instead of through molecular recognition as in self-assembly which is an equilibrium process [1]. The self assembly process involves molecular recognition between fundamental building blocks. Self assembly is dynamic, the final product of materials that are self-assembled via molecular recognition can change due to fundamental changes in the units or environment [4].

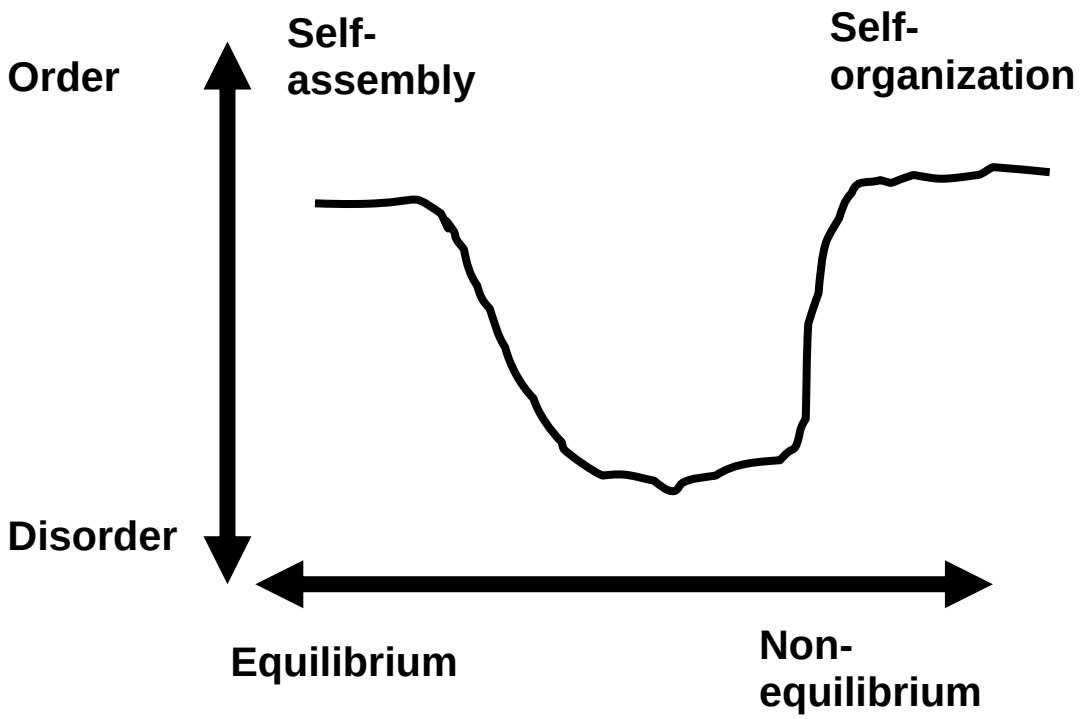

Figure 1.2: Schematic of Self-assembly and Self-organization

Beta-amyloid peptides are a sequence of amino acids that self-assembles into various structures depending on the length of the sequence, pH, temperature, and solution [5-7]. The Lynn group has invested much time in understanding the self assembly process of truncated segments of Aβ(1-42). Time and patience has led to the discovery of Aβ peptide nanotubes which vary in size based on environmental conditions [5, 7, 8]. It is with these novel peptide nanotubes that I seek to understand potential applications through the encapsulation of small molecules.

References

1. Roco, M., Morrison Mark, Malsch Ineke, Yamamoto, Kenji, *Biomedical Nanotechnology*. Taylor & Francis: 2005; p 209.
2. Ishijima, A. a. Y., T. , Single Molecule Nanobioscience. *Trends Biochemical Science* **2001,** 26, 438-444.
3. Foster, L. E., *Nanotechnology Science, Innovation, and Opportunity*. Prentice Hall: 2006; p 283.
4. Zhang, S., Marini,D, Hwang,W, and Santoso,S., Designing Nanobiological Materials through Self-Assembly of Peptides and Proteins. *Current Opinion in Chemical Biology* **2002,** 6, 865-871.
5. Morgan, D. M. L., D.G.; Lakdawala, A.S. Snyder, J.P.; Liotta,D.C., Amyloid Structure: models and theoretical considerations in fibrous aggregates. *J. Chin. Chem. Soc.* **2002,** 49, (459-466).
6. Lu, K.; Jacob, J.; Thiyagarajan, P.; Conticello, V. P.; Lynn, D. G., Exploiting amyloid fibril lamination for nanotube self-assembly. *Journal of the American Chemical Society* **2003,** 125, (21), 6391-3.
7. Dong, J. J.; Shokes, J. E.; Scott, R. A.; Lynn, D. G., Modulating amyloid self-assembly and fibril morphology with Zn(II). *Journal of the American Chemical Society* **2006,** 128, (11), 3540-3542.
8. Lu, K. Discovery of Diversie Peptide Nanotube Architecture form the Self-assembly of Designed Amyliod-β Cassettes. Emory University, Atlanta, 2006.

Chapter 2

Bilayer Stability

Amyloid fibers are able to self assemble in vitro from different polypeptides and proteins which are involved in many of the diseases that were listed in Chapter 1 [2]. It has been discussed that when amyloid fibers aggregate, they are very stable and difficult to solubilize [14]. I have decided to study shorter sequences of the amyloid assembly of polypeptides [1-3]. The Aβ (16-22) is the shortest sequence of the amyloid plaque that is soluble and well studied [4]. This sequence Aβ (16-22) has the alternating hydrophobic/hydrophilic repeating sequence as shown in Figure 2.1 [4].

^{1}DAEFRHDSG^{10}YEVHHQKLVF^{20}FAEDVGSNKG^{30}AIIGLMVGGV^{40}VIA

Figure 2.1: Aβ(1-42) Red indicates predominately hydrophobic and blue indicates predominately hydrophilic residues.

Structural studies have suggested that synthetic amyloid fibrils are composed of a core beta sheet structure in which the beta strands run orthogonal to the fiber axis and that the frequent and repetitive hydrogen-bonding extends parallel to the fiber axis [11]. The formation of fibers are proposed to form through a nucleation-dependent pathway as shown in **Figure 2.2** [5]. It has been proposed that the model assembly of amyloid fibers occurs through an observed lag time and seeding effect with fibers [6, 7]. The model shows monomers going through a series of associations (lag time) to associate in an oligomeric nucleus. This step is then followed by a growth step that forms larger polymers. The last step consists of the monomers and polymers in equilibrium [8]. **Figure 2.2** shows that there is no assembly under the critical concentration and the seeding effect is necessary

for polymerization [8]. This observation is also seen in peptide micelles a critical concentration is seen and then a nucleation step [9].

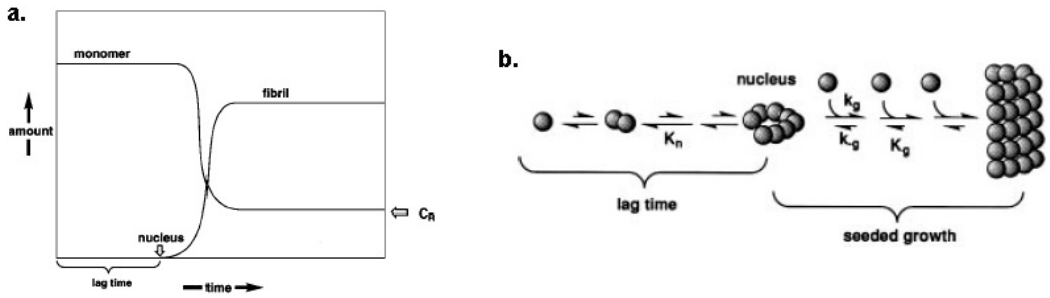

Figure 2.2: Nucleation-dependent pathway to form fibers.

Amyloid fiber growth proceeds through a nucleation-dependent pathway as shown in **Figure 2.2** [5]. There are several factors that contribute to the formation of fibers including: peptide sequence, concentration, pH, solvent, ionic strength, temperature and other solutions [8]. The beta sheets are arranged parallel along the fiber axis and this is due to the hydrogen bonding network [11]. The amyloid fibers are thought to be composed of two or more beta sheets held together by hydrophobic surface contacts or specific electrostatic interactions [13]. The stabilization of the beta sheet is due to the overlay of hydrophobic and hydrophilic side chains [12]. The amyloid beta sheets is sequence sensitive as mutating one of the amino acids with proline it disrupts the beta sheet [1].

Seprell *et al.*(2005) designed an amino acid sequence (KFFEAAAKKFFE) to probe the structure of amyloid fibers. The aforementioned peptide was crystallized and by x-ray diffraction, the crystals diffracted to high resolution (1Å) by electron and x-ray diffraction [1]. Their findings show that the β-sheets are antiparallel and held together by π-bonding between phenylalanine rings and salt bridges between glutamic acid and lysine pairs which contribute to stabilization. The β-sheets are arranged in the signature cross β

sheet arrangement. X-ray diffraction data have shown Aβ fibrils to have reflections at 4.7Å and 10.6Å [10]. The reflections were fit to a cross beta sheet structure with the 4.7Å reflecting the H-bonding between strands and the 10.6Å reflecting the stacking (lamination) distances between beta- sheets [11, 12].

The use of solid-state (ss) NMR has become the technique of choice to investigate the structural dimensions of the Aβ fibrils [13]. Solid state NMR was used to measure the interstrand distances of Aβ (10-35) via ^{13}C labeling of the carbonyls [13]. **Figure 2.3** shows that the interstrand distances measured for the fibers show that the peptides were parallel and in register [1]. Coupling the ss-NMR data with small angle and neutron scattering a model (**Figure 2.3a, 2.3b, 2.3c**) was developed. The model has six beta sheets laminated in a parallel in-register arrangement [1].

a.

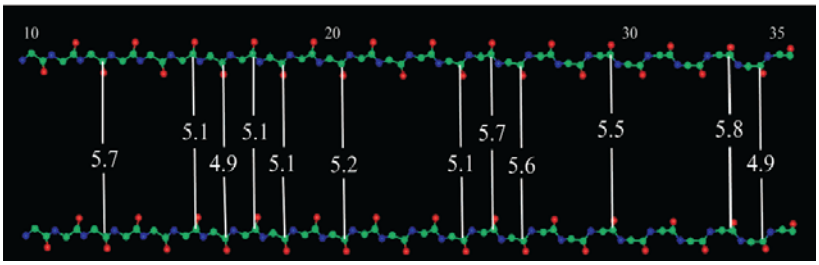

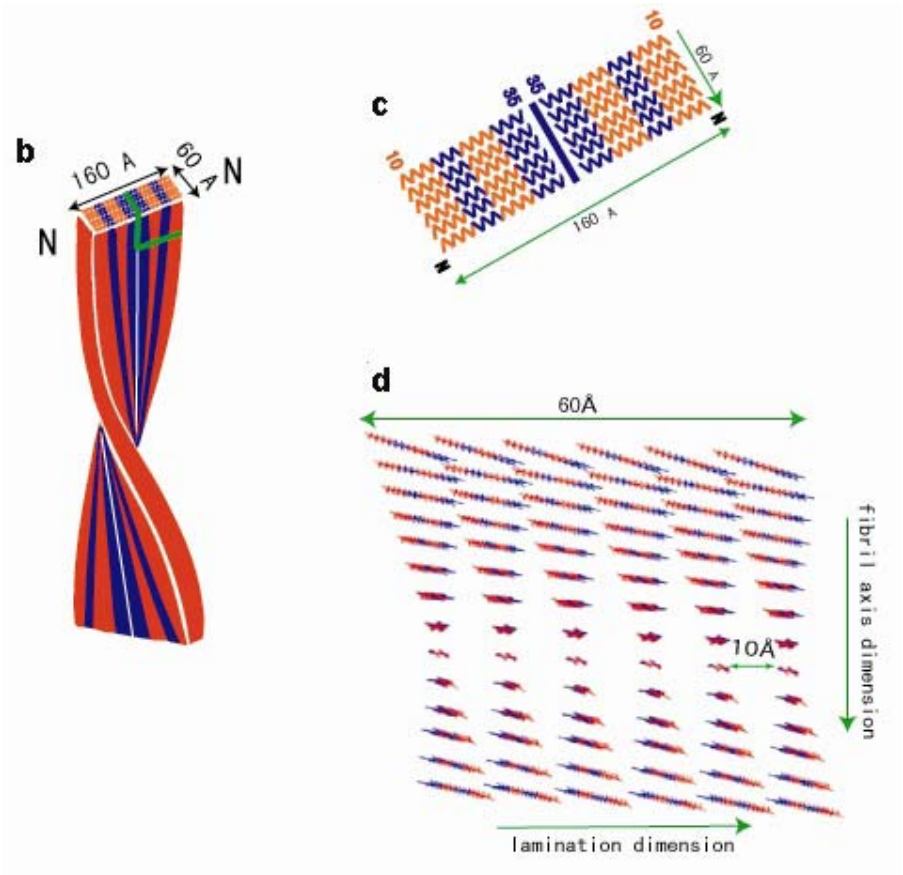

Figure 2.3a-d:
Structural Model for Aβ (10-35): (b) The red color represents hydrophilic regions and the blue color represents hydrophobic regions of the paired Aβ (10-35) fibril model with; (c) the top view of the fibril resembles a peptide bilayer; (d) six β-sheets laminates show the side view of the fibril [8].

The amyloid fibrils can adopt an array of structures: parallel, antiparallel, or folded [8]. These arrangements are based on inter and intra molecular interactions of the sidechains [14, 15]. This information coupled with molecular dynamics (MD) simulations led to the discovery of peptide nanotubes [16, 17].

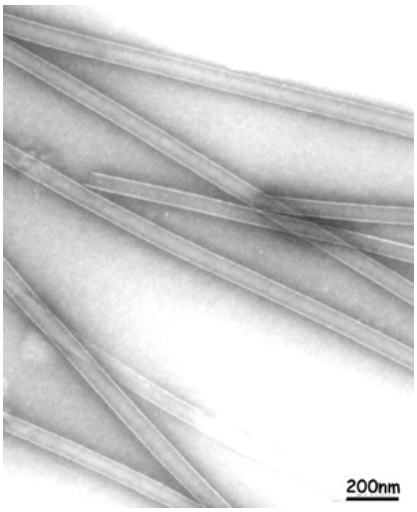

Figure 2.4: TEM image of Aβ (16-22) peptide nanotubes ~80nm [8].

The increase in laminates are from six laminates in Aβ (10-35) fibers to 130 laminates in Aβ (16-22) peptide nanotubes [8]. As the number of laminates increase the diameter increases, which results in peptide nanotubes [8].

The stabilization of fibers is due to the dynamic nature of the hydrogen bonds between laminates [8]. Aβ (16-22) can self assemble in acidic conditions to form homogeneous peptide nanotubes [8]. Small Angle X-ray scattering (SAXS) data confirm that the TEM of peptide nanotubes are hollow cylindrical tubes. **Figure 2.4** shows a scattering profile (open circles) the red curve is the fit to the Aβ (16-22) scattering data with a hollow cylinder form-factor. With this form-factor the solution SAXS data is consistent with an outer diameter of 52nm and wall thickness of 4nm.

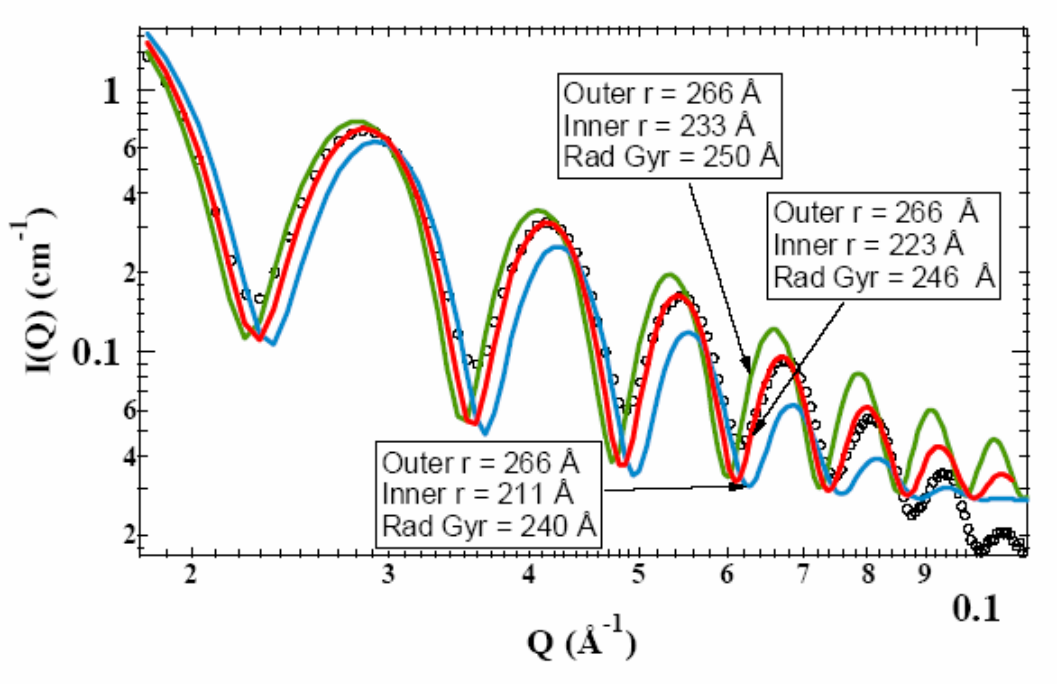

Figure 2.5: Small Angle X-ray Scattering (SAXS) Profile

The SAXS data show the calculated curves for a nanotube and a solid cylinder with the same outer radius. **Figure 2.5** compares the actual fit (red curve) with a solid cylinder with the same outer radius (green curve). The red curve best fits the data (open circles) [8].

The model in **Figure 4.2** was generated by data from: TEM, AFM, SAXS, and SANS. The backbone spacing at 5 Å is determined by the backbone H-bonds between adjacent peptides, which are on the long axis of each sheet[3, 8]. Therefore this fixes a peptide between adjacent parallel, in register β-strands[3, 8]. The 10 Å spacing between the individual anti-parallel β-sheets defines the lamination dimension [3, 8]. The Aβ(16-22) assemblies into peptide nanotubes at relatively low concentrations (1.5mM). These peptide nanotubes can interact with citrate coated gold nano particles which are negatively charged [8]. This leads to the hypothesis that these nanotubes could interact with negatively charged DNA.

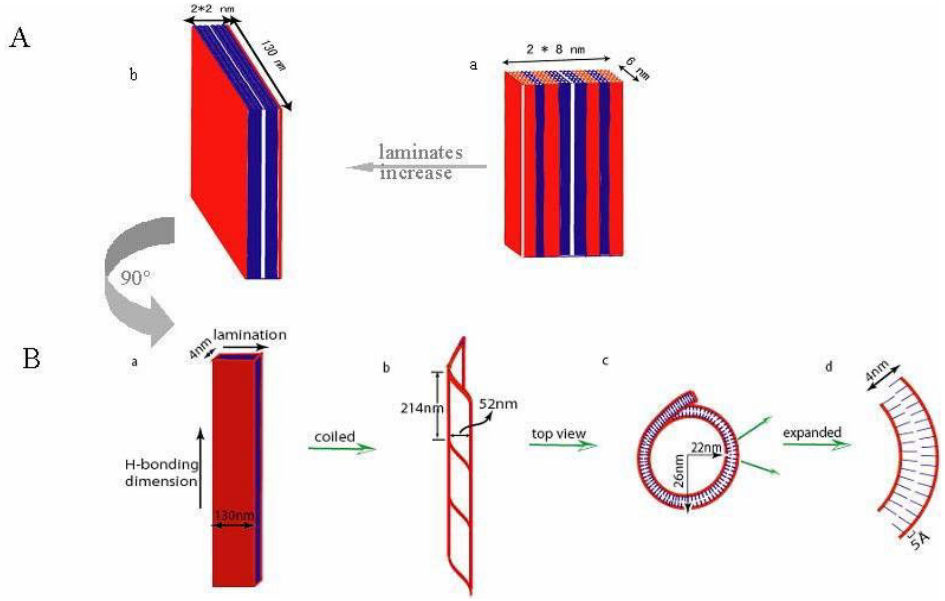

Figure 2.6: Model of Aβ (16-22) peptide nanotubes.

A. Bilayer model to Aβ (10-35) fibril. The lamination increased from 6nm to 130 nm after shortening the peptide length. B. (a) A rectangular bilayer, 130 nm wide by 4 nm thick, with each leaflet composed of β-sheets, and the corresponding backbone H-bonds, oriented on the long axis, and β-sheet lamination defining the 130 nm bilayer width. (b) The coiled tubular fibril with an outer diameter of 52 nm and an outer helical pitch of 214 nm. (c) Top view of the 44 nm internal cavity. (d) Amplified view of the wall with a thickness of 4 nm and the distance between each anti-parallel β-strand being the backbone H-bond distance of 5 Å [8].

In Chapter 1 the use of peptide nanotubes as DNA encapsulation devices were introduced, which requires physiological conditions (neutral pH). Aβ(16-22) assembles

into a heterogeneous mixture of nanotubes and fibers in phosphate buffer which are ideal conditions for DNA encapsulation. However the heterogeneity of the system structures is not ideal when exploring possible delivery devices. Lu found by changing the solvent to acetonitrile, fibers formed at neutral pH and nanotubes formed at acidic pH [8]. This work led her to discover that the C-terminal position controlled not only morphology but the stability of the peptide nanotube at neutral pH [8]. Mutation studies have been conducted on the C-terminus of the Aβ (16-22) sequence in water at pH2 and show that the C-terminus is critical in the formation of peptide nanotubes [8]. The Aβ (16-22) C-terminus is located in a critical β-sheet region where hydrophobic interactions play an important role in the assembly of peptide nanotubes [8]. The following hydrophobic residues at the C-terminus can form nanotubes: F, L, M, V, and W [8]. The hydrophilic residues without charge that can form nanotubes are: G, Q, S, and T [8].

However changing the solvent conditions to pH 2 40% acetonitrile/water, Aβ (16-22) self assemblies into various morphologies (nanotubes, sheets, fibrils, and no assemblies) depending on the C-terminus residue [8]. These observations were monitored by Circular Dichroism (CD), Transmission electron microscopy (TEM), and Atomic force microscopy (AFM) [8].

E22G (KLVFFAG) mutants are able to self assemble readily in pH 7 water [8]. The previous chapter introduced current technologies that are investigating ways to either enclose genetic information or transport materials in nanoscale structures. The E22G mutant was investigated as a potential carrier of genetic information. The homogenous peptide nanotubes have a positive charge due to the N-terminal lysine. The positive charge on the surface of the peptide nanotubes is complementary to the negatively

charged DNA. Therefore this electrostatic interaction was investigated with the E22G peptide nanotube.

Method

Peptide Nanotube Synthesis:

The seven residue peptide mutant Aβ (16-22) E22G, CH_3CO-KLVFFAG-NH_2, was synthesized with standard FMOC solid phase procedures with both N and C termini capped. The monomer was dissolved in de ionized water and adjusted to pH 7 with 0.1M NaOH and incubated for 24 hours at room temperature. Figure 7.2 below is a circular dichroism spectra of a 3mM E22G incubated for 24hours at pH 7.

E22G and DNA mixing Experiment

Mature 3mM E22G peptide nanotubes were assembled in de ionized water and adjusted to pH 7 with 0.1M NaOH. The following DNA sequences (there was no specific reason for the monomers that were chosen) were ordered from Sigma Genosys:

24 monomer sequence (5'-3'), desalted, and on 1.00 scale

5'CTCGTCTGGCAGGCGACGGCTC 3' *abbreviated (DB-E22G-CTC)*

3'GAGCAGACCGTCCGCTGCCGAG 5'*abbreviated (DB-E22G-GAG)*

Circular Dichroism

Samples were prepared and performed by established Circular Dichrosim procedures [8]. A quartz cuvette with a 0.1 mm path length was used with 17 µl of solution. The spectra was scanned between 260 nm to 190 nm with a scanning rate of 100 nm/min with a resolution of 0.2 nm with a Jasco J-810 spectropolarimeter. Three wavelength scans were averaged together with the buffer control subtracted.

Transmission Electron Microscopy (TEM)

10 µl of E22g was applied to TEM grids (Formvar/carbon film coated 200 mesh) and allowed to absorb for 1 min. The peptide solution was wicked off with filter paper. 2% uranyl acetate was placed on the grid for 3 minutes and wicked off with filter paper. The grids were placed under house vaccum overnight. The TEM micrographs were taken on a Hitachi H -7500 transmission electron microscope instrument.

Results and Discussion:

TEM micrographs confirmed that the 3mM E22G sample of peptide, assembled into tubular structures. Sharp white edges as seen for Aβ(16-22)**,** were seen for the 3mM E22G sample are consistent with a hollow tubular structure that was stained with uranyl acetate.

Initial work was conducted to investigate the interactions of 3mM E22G in pH 7 water with deoxyribonucleic acid (DNA). The hypothesis was that the DNA would be attracted to the E22G nanotube due to cooperative electrostatic interactions. The electrostatic interactions would arise from the positively charged surface of the nanotube via the solvent exposed lysines and the negative charge of the DNA from the phosphate backbone. By performing mixing experiments with mature E22G peptide nanotubes with single and double stranded DNA we can begin to investigate the way(s) in which DNA can interact with these Nanoscale structures.

Experiments were monitored by Circular Dichroism (CD) and Transmission Electron Microscopy (TEM) to note any signature or morphological changes respectively. The CD exhibited the typical β-sheet signature. However the TEM

images revealed an interesting observation. Upon the addition of DB-E22G-GAG there were noticeably fragmented and/or shorten peptide nanotubes.

a.

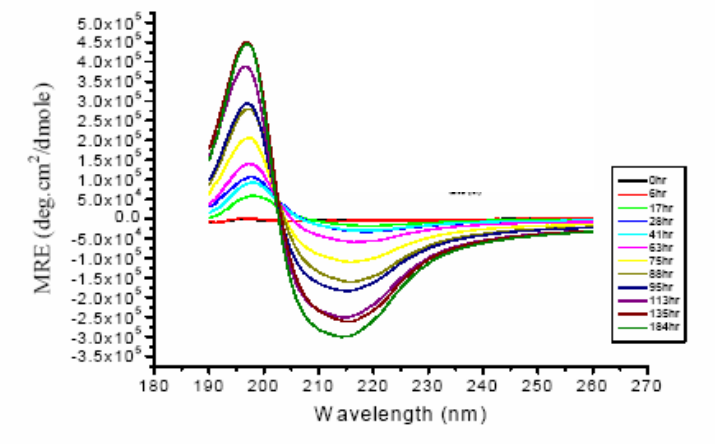

b.

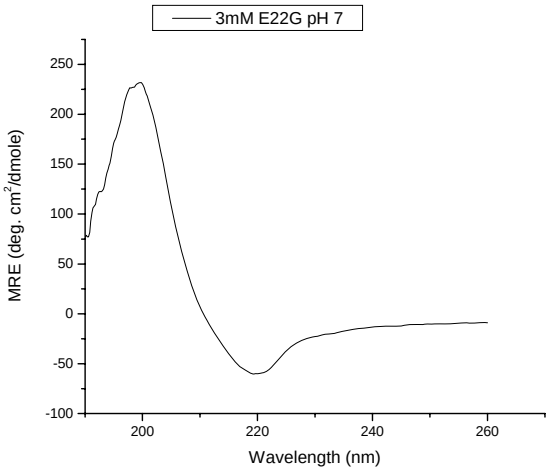

Figure 2.7: CD spectra of a. Aβ(16-22) wild type [8] and b. Aβ(16-22) E22G. (a) 1.3 mM Aβ(16-22) dissolved in 40% acetonitrile/water with 0.1%TFA (pH 2). CD monitored from 0hrs to 184hrs. (b) A β-sheet signature develops over 24hrs. Mature peptide nanotubes have a positive ellipticity at ~195nm and a negative ellipicity at ~215nm [8].

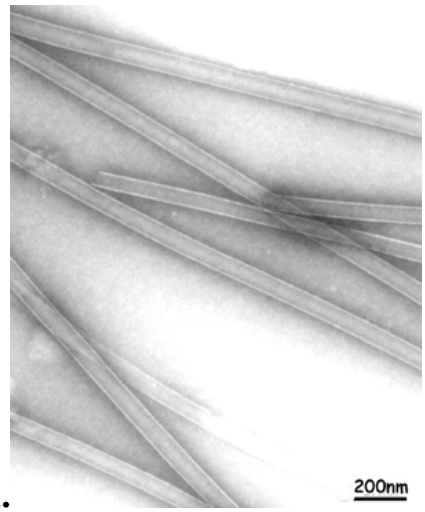

a.

Figure 2.8: (a) Transmission Electron Micrograph of Aβ (16-22) [8].

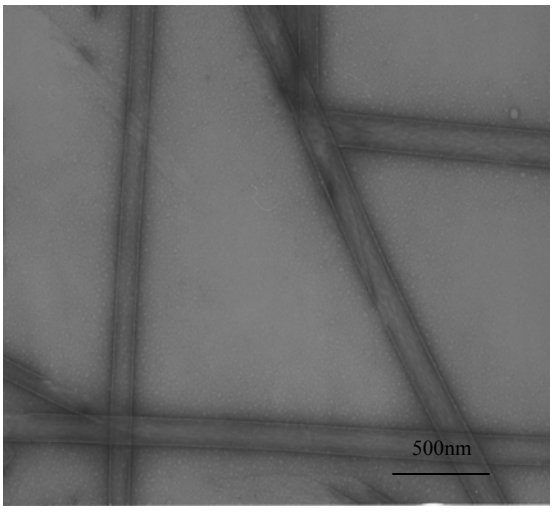

b.

Figure 2.8: (b) Transmission Electron Micrograph of Aβ (16-22) E22G in pH 7 water.

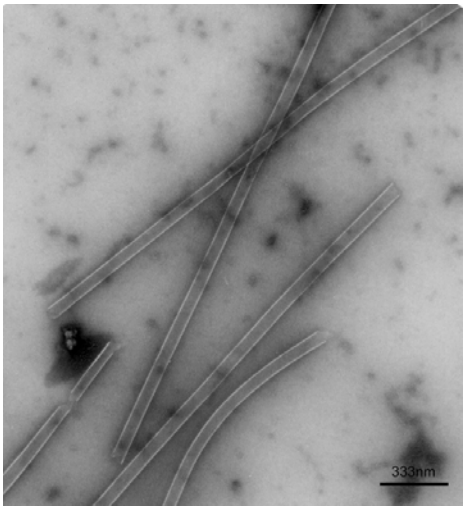

Figure 2.9: (a) TEM micrograph of E22G mixed with DNA. Smaller pieces are fragments of E22G peptide nanotube.

This experiment was analyzed by conducting experiments with Adenine, Adenosine Monophosphate and sodium phosphate. Adenine would test the effect(s) of a nucleobase without a charge on E22G. Adenosine Monophosphate has a negative charge and the aromaticity from the nucleoside. The sodium phosphate was chosen to investigate how a single negative charge affects E22G. The experiments were performed at a 1: ~3 ratio of E22G peptide concentration to small molecule (Ad, AMP, Na_2HPO_4) concentration. Circular Dichroism shows (**Figure 2.10**) that after adding Adenine (Ad) ,Adenosine Monosphophate (AMP), and disodium phosphoric acid (Na_2HPO_4) that the intensity of the β-sheet signature decreased. The positive ellipicity ~195 and the negative ellipicity ~215 decreases could be interrupted as a decrease in β-sheet signature, hence the peptide nanotube population. The population of peptide nanotubes was shorter as shown via transmission electron micrographs (**Figure 2.10**). Additional studies were conducted to observe the dilution effects of the 3mM E22G peptide nanotubes. Circular

Dichroism studies show that upon dilution of the 3mM E22G peptide nanotubes there was a decrease β-sheet signature.

Conclusion

E22G peptide nanotubes were chosen because of their ability to form at pH 7 in water. However, mixing preformed E22G tubes with Phosphate, Adenine, Adenosine Monophosphate and a 24-mer DNA strands indicated that, the E22G peptide nanotubes was not stable. Initially the hypothesis for the fragmentation of the peptide nanotubes, was due to the addition of the small molecules. **Figure 2.12** shows that as E22G peptide nanotubes were diluted, the stability of the peptide nanotube was compromised leading to the destabilization of the nanotubes. In the E22G peptide nanotube, the critical concentration (**Figure 2.2**) is needed to drive assembly to nanotubes. The glycine mutation, a flexible residue at the C terminus, shows that is important to form homogeneous stable nanotubes at the 3mM concentration [8]. However, diluting the system below the critical concentration disturbs the stability of the bilayer. The bilayer model isn't stable to use in investigating how small molecules interact with peptide nanotubes. A system must be stable upon dilution, the CyCy peptide nanotube is a monolayer system. The monolayer peptide nanotube doesn't require the critical concentration that is seen in E22G. The CyCy monolayer nanotube is driven by molecular recognition of the modified nucleobases between laminates [18]. It is with this understanding that I will investigate how small molecules interact with CyCy peptide nanotubes.

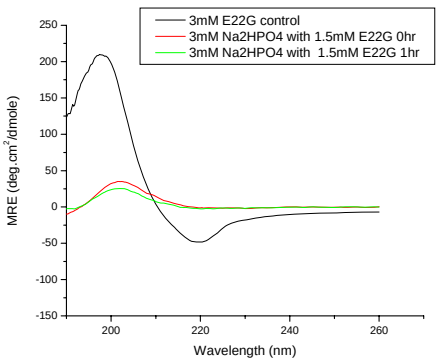

a.

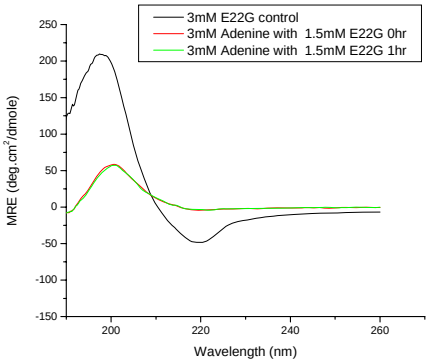

b.

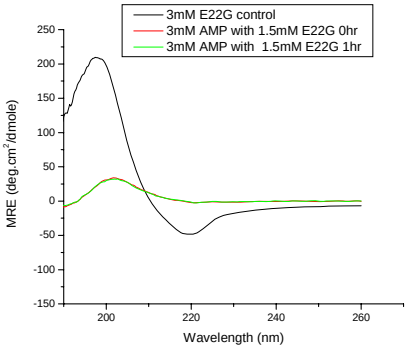

c.

Figure 2.10a-c: Circular Dichroism Mixing Experiment (a) 3mM E22G control (black), 1.5mM E22G with 3mM Na2HPO4 at 0hr (red), 1.5mM E22G with 3mM Na2HPO4 at 1hr (green); (b) 3mM E22G control (black), 1.5mM E22G with 3mM Adenine (red), 1.5mM E22G with 3mM Adenine at 1hr (green); (c) 3mM E22G control (black), 3mM AMP with 1. 5mM E22G 0hr (red), 3mM AMP with 1.5mM E22G at 1hr (green).

a. 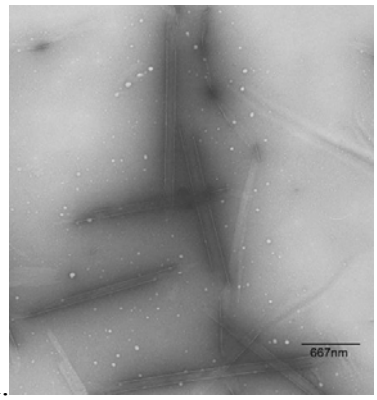

b. 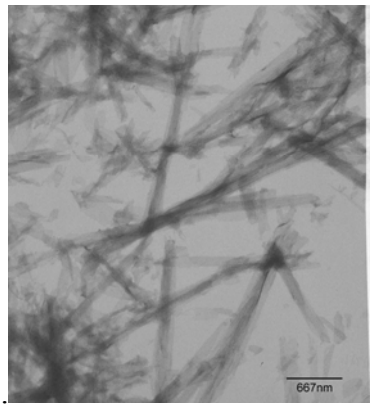

c. 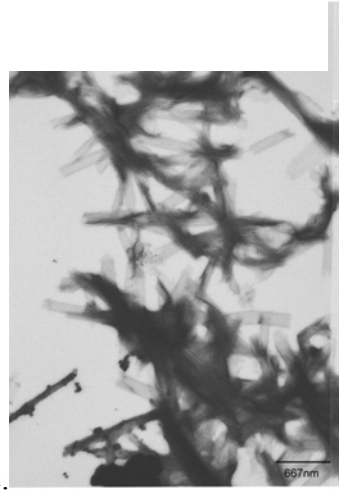

Figure 2.11 a-c: Transmission Electron Micrographs: (a) 3mM Adenine with 1.5mM E22G the nanotubes are not homogeneous in morphology a mixture of fragmented nanotubes and fibers. (b) 3mM Adenosine Monophosphate with 1.5 mM E22G the nanotubes morphology changed to unraveled nanotubes/sheet structures. (c) 3mM Na2HPO4 with 1.5 mM E22G this micrograph shows shorter nanotubes that aggregated.

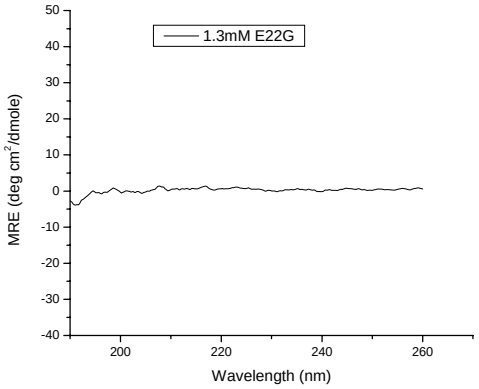

a

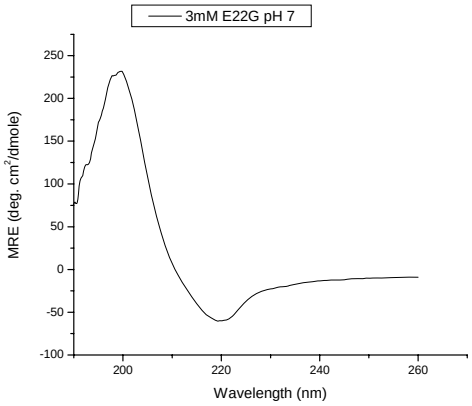

b.

Figure 2.12 a-b: (a) CD spectra of E22G diluted from 3mM concentration to 1.5mM concentration. (b) 3mM E22G peptide nanotube showing the typical β-sheet signature.

References

1. Burkoth, T. S.; Benzinger, T. L. S.; Urban, V.; Morgan, D. M.; Gregory, D. M.; Thiyagarajan, P.; Botto, R. E.; Meredith, S. C.; Lynn, D. G., Structure of the beta-amyloid((10-35)) fibril. *Journal of the American Chemical Society* **2000,** 122, (33), 7883-7889.
2. Dong, J. J.; Shokes, J. E.; Scott, R. A.; Lynn, D. G., Modulating amyloid self-assembly and fibril morphology with Zn(II). *Journal of the American Chemical Society* **2006,** 128, (11), 3540-3542.
3. Lu, K.; Jacob, J.; Thiyagarajan, P.; Conticello, V. P.; Lynn, D. G., Exploiting amyloid fibril lamination for nanotube self-assembly. *J Am Chem Soc* **2003,** 125, (21), 6391-3.
4. Kang, J. L., H.G.; Unterbeck, A.; Salbaum, J.M.; Masters, C.L.; Grzeschik, K.H.; Multhaup, G.; Beyreuther, K.; Muller-Hill, B. , The Precursor of Alzheimer's Disease Amyloid A4 Protein resembles a Cell-Surface Receptor. *Nature* **1987,** 325, 733-736.
5. Harper, J. D. L., P.T., Jr. , Models of amyloid seeding in Alzheimer's disease and Scapie: Mechanistic truths and physiological consequences of teh time-dependent solubility of amyloid proteins. *Annu Rev Biochem* **1997,** 66, 385-407.
6. Harper, J. D. W., S.S.; Lieber, C.M.; Lansbury, P.T. Jr. , Assembly of A beta amyloid protofibrils: an in vitro model for a possible early event in Alzheimer's disease. *Biochemistry* **1999,** 38, 8972-8980.
7. Jarrett, J. T. B., E.P.: Lansbury, P.T.Jr, The carboxy terminus of the beta amyloid protein is critical for the seeding of amyloid formation: implications for the pathogenesis of Alzheimer's disease. *Biochemistry* **1993,** 32, 4693-4697.
8. Lu, K. Discovery of Diversie Peptide Nanotube Architecture form the Self-assembly of Designed Amyliod-β Cassettes. Emory University, Atlanta, 2006.
9. Lomakin, A. C., D.S.; Benedek, G.B.; Kirschner,D.A.; Teplow, D.B., On the nucleation and growth of amyloid beta-protein fibrils: Detection of nuclei and quantitation of rate constants. *Proc Natl Acad Sci U S A* **1996,** 93, 1125-1129.
10. Serpell, L. C., Alzheimer's amyloid fibrils: Structure and Assembly. *Biochim. et Biophys. Acta* **2000,** 1502, 16-30.
11. Fraser, P. E. N., J.T.; Surewicz, W.K.: Kirschner, D.A., pH-dependent Structural transitions of Alzheimer Amyloid Peptides. *Biophys J* **1991,** 60, 1190-1201.
12. Inouye, H.; Nguyen, J. T.; Fraser, P. E.; Shinchuk, L. M.; Packard, A. B.; Kirschner, D. A., Histidine residues underlie Congo red binding to A beta analogs. *Amyloid* **2000,** 7, (3), 179-88.
13. Spencer, R. G. H., K.J.; Auger, M.; McDermott, A.E.; Griffin, R.G.; Lansbury, P.T. Jr, An unusual peptide confromation may precipitate amyloid formation in Alzheimer's disease: application of solid-state NMR to the determination of protein secondary structure. *Biochemistry* **1991,** 30, 10382-10387.
14. Hilibich, C. K.-W., B.; Reed, J.; Masters, C.L.; Beyreuther, K., Aggregation and Secondary structure of synthetic amyloid beta A4 peptides of Alzheimer's disease. *J. Mol. Biol* **1991,** 228, (460-473).

15. Hilibich, C. K.-W., B.; Reed, J.; Masters, C.L.; Beyreuther, K., Substitutions of hydrophobic amino acids reduce the amyloidogenicity of Alzhemier's disease beta A4 peptides. *J. Mol. Biol* **1992,** 228, (460-473).
16. Lakdawala, A. S. M., D.M; Liotta,D.C.; Lynn,D.G; Snyder,J.P., Dynamics and Fluidity of Amyloid Fibrils: A Model of Fibrous Protien Aggregates. *J. Am. Chem .Soc.* **2002,** 124, (15150-15151).
17. Morgan, D. M. L., D.G.; Lakdawala, A.S. Snyder, J.P.; Liotta,D.C., Amyloid Structure: models and theoretical considerations in fibrous aggregates. *J. Chin. Chem. Soc.* **2002,** 49, (459-466).
18. Liu, P. Modulating Amyloid Peptide Self-Assembly with Nucleobase Incorporation. Emory University, Atlanta, 2007.

Chapter 3

Small Molecule Interaction

The goal of this work is to find a delivery vehicle to encapsulate small molecules. In Chapter 2 the initial peptide nanotube, E22G, was found not to be stable upon dilution. The stability of the delivery vehicle is vitally important to potentially encapsulate small molecules. We have also found that other segments of the Aβ (1-42) can self assemble into nanotubes with the addition of metals and nucleobases [1, 2]. Aβ (13-21) ,HHQKLVFFA, was shown to self assemble into peptide nanotubes, when lysine was mutated to alanine and the addition of Zn^{2+} [3]. The histidine dyad is proposed to be the metal biding site [4, 5]. In Aβ (13-21)K16A, Zn^{2+} chelates to Histidine 13 in one peptide and the parallel in register Histidine 14 in a corresponding peptide [6]. The zinc chelation stabilizes the lamination dimension which causes an in the number of laminates [3]. **Figure 3.1** illustrates the lamrination and fibril axis of Aβ (13-21)K16A with zinc.

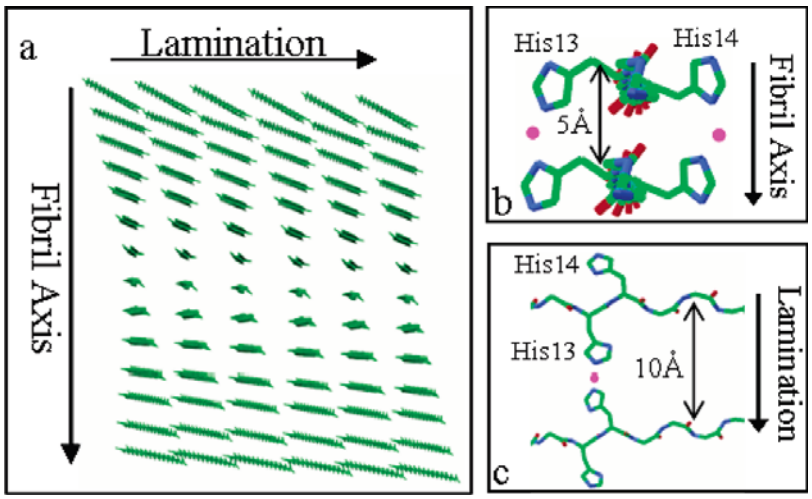

Figure 3.1 a –c: a) Shown is a five laminate fibril with six β-sheets consisting of β-strands that hydrogen bond parallel to the fibril axis. b) Shown is potential zinc binding sites of two peptides 5 Angstroms apart along the fibril axis. c) Potential zinc binding sites between two beta strands along the lamination dimension. [3]

Dong et. al. found by having a peptide, Aβ (13-21)K16A, to zinc ratio of 0.6-0.8 and allowing the structures to incubate, tubular structures formed having a diameter between 200-300nm [3]. In contrast Aβ (13-21)H14A forms fibers, these studies suggest that the histidine dyad is important for zinc chelation and lamination growth [3]. The zinc data shows that molecular recognition between sheets is important for increased lamination growth for tube formation.

It was hypothesized that inserting a modified cytosine into the Aβ (13-21)K16A in place of the histidines 13 and 14, could strengthen the lamination growth due to base pairing of the cytosines. Molecular Dynamics simulations studies of Aβ (10-21), replacing H13 and H14 histidine sidechains with β(cytosine-1-yl) alanine (**Figure 3.2**) shows that the cytosines could fit within the necessary 10Å laminate distance [2].

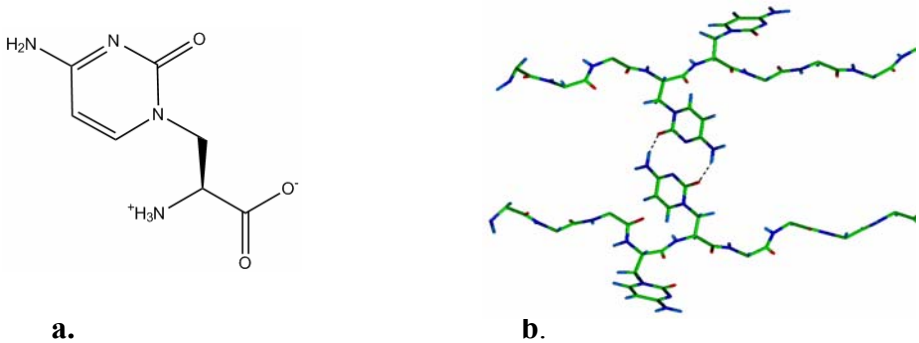

a. **b**.

Figure 3.2 a-b: a) β (cytosine-1-yl) alanine. b) Proposed hydrogen bonds (dashed lines) between modified Cy13 and Cy14 side chains residing in two extended β-sheets (model predicted by SYBYL in Aβ(10-21) Distance between peptide backbone is ~10Å [2, 7].

Figure 3.2b is a snapshot of the SYBYL computational modeling. The molecular dynamic simulations lead to the design of nucleobase peptide nanotubes. Transmission electron microscopy (TEM) shows that Aβ(13-21)K16AH13CyH14Cy (CyCy peptide) forms homogenous peptide nanotubes between pH 3.3 and 4.3 (**Figure 3.3**) [2]. The peptide nanotubes were proven to be hollow by Single Angle X-ray Scattering (SAXS) fitting [2].

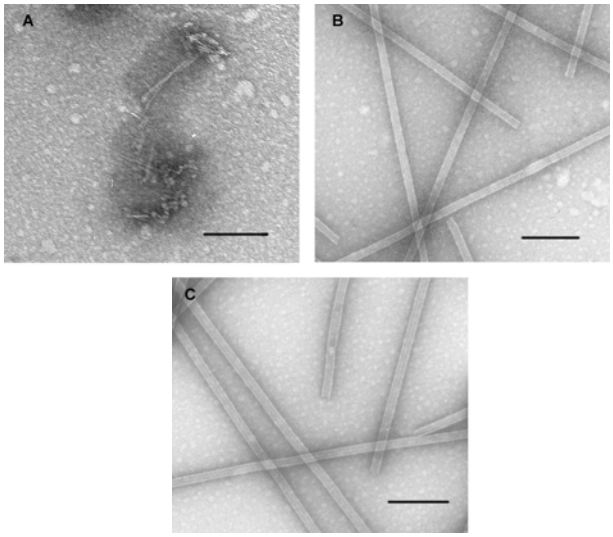

Figure. 3.3 A-C) 0.3mM Peptide in 25mM MES buffer and adjusted to different pH (A: pH2.0, B: pH3.3, C: pH4.3). At pH3.3 and pH4.3, which is around the pKa of cytosine, Aβ(13-21)CyCy forms homogenous tubular structure. At pH2.0, only particles and thin filaments are formed. At pH5.5 (not shown), fibrils co-exist with tubes. Scale: 200 nm. [2]

Transmission electron micrographs (**Figure 3.3 A**) show that at low pH (pH 2.0) self-assembly occurs, but only into thin filaments and particles. However with an increase in pH, shown in images B and C, tubular structures are observed. Therefore, pH appears to be critical for Aβ(13-21)K16AH13CyH14Cy to assemble into tubes. The pKa of cytosine is 4.5 and laminate stabilization is achieved near the pKa of ctosine which causes a hemi protonated state of the cytosines. SAXS data show that the hollow cylinders have an outer radius of 12.7nm and a wall thickness of 3.8nm. These observations suggest that hemi-protonated, H-bonded cytosines stabilize the laminate dimension, which favors an increased number of laminates, hence leading to the

formation of tubes. **Figure 3.4** is a model of the Aβ (13-21)K16AH13CyH14Cy peptide nanotube [2].

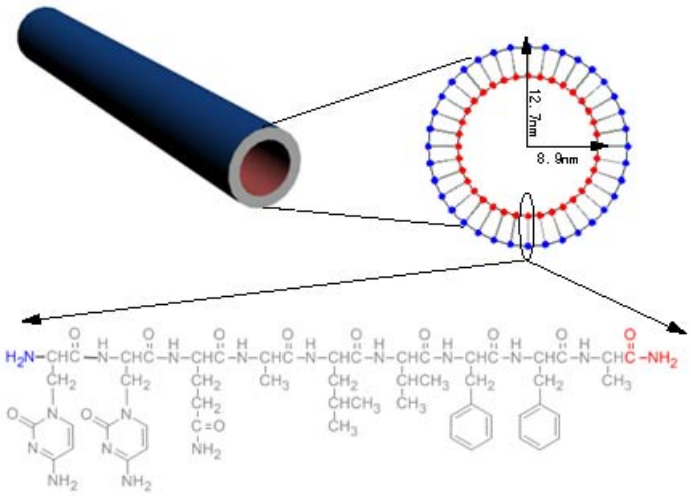

Figure 3.4. Model of the nucleobase peptide nanotube (the N-terminus, blue, is with out a capping group and the C terminus, red, is capped).

Studies have been conducted to determine location of cytosines with respect to the tubes, by reducing Ag^+ with $NaBH_4$ in the presence of Aβ (13-21)K16AH13CyH14Cy peptide nanotubes. Ag^+ coordinates with heterocyclic bases and we anticipate seeing the colloidial particles coating the tubes surfaces. Transmission electron micrograph (**Figure 3.5**) shows silver particles coating the surface Aβ(13-21)K16ACyCy. This data suggest that there silver is interacting with the peptide nanotube however it does not distinguish if colloidial particles are on the outside or inside. These studies are consistent with small molecules interacting with the CyCy nanotubes with the tubes remaining intact. The remainder of this chapter will investigate if CyCy nanotubes are sutiable for use as delivery vehicles and specifically investigate the interaction with AMP as well as

investigate the possibility of using other nucleobases to create nucleobase peptide nanotubes.

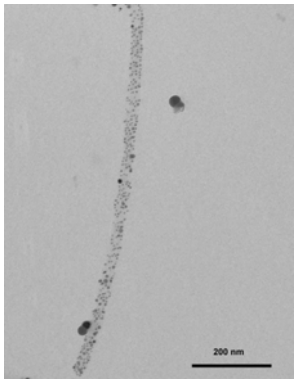

Figure 3.5: TEM image of CyCyQALVFFA nanotubes coated with silver.

The proposed monolayer nucleobase peptide nanotubes are stable upon dilution. This system is a good candidate to be investigated as a potential delivery vehicle. The following data

Methods:

Nucleobase Peptide Nanotube Synthesis

N-(9-Fluorenylmethoxycarbonyl)-β-(cytosine-1-yl)alanine synthesis [8-10] .

Synthesis of N-(9-Fluroenylmethoxycarbonyl)-β-(cytosine-1-yl)alanine

N-(tert-Butoxycarbonyl)-L-serine β-lactone (1) [9]

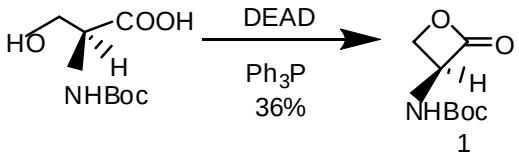

N-(tert-Butoxycarbonyl)-L-serine (6.2 g, 30 mmol) and triphenylphosphine (7.9 g, 30 mmol) was dissolved in 200 ml anhydrous tetrahydrofuran under nitrogen and cooled to -78 ºC. Diethyl azodicarboxylate (6.3 g, 30 mmol) 5.7 mL was added dropwise. The reaction stirred overnight. The solvent was removed by rotoevaporation. The reaction

mixture was purified by flash column packed in hexane. The solvent was changed to hexane/ethyl acetate (65/35) gradually. The β-lactone was readily visualized by TLC (hexane/ethyl acetate (65/35) as solvent system, R_f ~0.44) by staining in iodine or potassium permanganate. **1** was isolated as a white solid (36%). mp 119.5-120.5 °C; ^{1}H NMR ($CDCl_3$, 400MHz) δ: 1.45 (s, 9H, $C(CH_3)_3$), 4.4-4.45 (m, 2H, CH_2), 5.05-5.15 (m,1H NH-C<u>H</u>), 5.15-5.25 (br s, 1H, NH); ^{13}C-NMR ($CDCl_3$, 400MHz) 28.0 ($C(\underline{C}H_3)_3$) , 59.8 (NH-CH), 66.9 (CH2), 81.9($\underline{C}(CH_3)_3$), 154.8 (NH-CO), 169.7(O-CO). IR (cm^{-1}) 3358, 1836, 1678, 1533, 1290, 1104. MS (CI) m/z $(M+H)^+$ 188.1 Calculated: 188.0923.

N_4-(Benzyloxycarbonyl)cytosine(5)

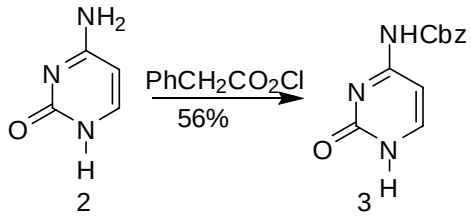

Benzyloxycarbonyl chloride (26 mL, 0.18 mol) was added dropwise to a suspension of cytosine (**2**) (10.0 g, 0.09 mol) in dry pyridine (500 mL) at 0 ºC under N_2. The mixture was stirred overnight and, the pyridine suspension was evaporated to dryness by rotoevaporation. Water (100 mL) was added and the pH was adjusted to 1 with 4 M HC1 (aqueous). The resulting white precipitate was removed by vacuum, washed with water, and partially dried. The wet precipitate was boiled with absolute EtOH (250 mL) for 10 min, cooled to 10 ºC, filtered, washed thoroughly with ether and dried, in vacuum and 3 was isolated as a white solid: yield 12.4 g (56%); mp > 250 ºC. ^{1}H NMR (DMSO-d_6, 400MHz) δ: 5.41(s, 2H, $CH_2(C_6H_5)$), 6.89 (d, 1H, HC(5)), 7.36 (m, 5H, (C_6H_5)), 7.76

(d, 1H, HC(6)). Anal. Calcd for $C_{12}H_{ll}N_3O_3$: C, 58.77; H, 4.52; N, 17.13. Found: C, 58.59; H, 4.55; N, 17.17.

N-(tert-Butoxycarbonyl)-β-(cytosine-1-yl)alanine 2 [9]

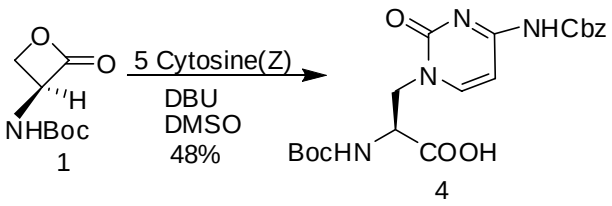

DBU (1.8 g, 12 mmol) was added to a suspension of N^4-(Benzyloxycarbonyl) cytosine (**3**) (2.5 g, 10 mmol) in DMSO (10ml). Within 15 min, a solution of N-(tert-Butoxycarbonyl)-L-serine β-lactone (2.2 g, 12 mmol) in DMSO (10 ml) was added. The mixture was stirred for 1h before the reaction was terminated with AcOH (686 μl, 12 mmol). The solvent was removed by rotoevaporation and the reaction mixture was purified by flash column packed in methylene chloride. The solvent was changed to methylene cholride/methanol (2/1) gradually. **4** was readily visualized by UV on TLC plate (methylene cholride/methanol (2/1) as solvent system, R_f ~0.49). **4** was isolated as a white solid (48%). ^{1}H NMR (DMSO-d_6, 400MHz) δ: 1.29 (s, 9H, $C(CH_3)_3$), 3.48/4.15 (2H, $H_2C(\beta)$), 4.45 (ddd, 1H, HC(α)), 5.13(s, 2H, $CH_2(C_6H_5)$), 6.35 (d, 1H, HN(BOC)), 6.86 (d, 1H, HC(5)), 7.32 (m, 5H, (C_6H_5)), 7.86 (d, 1H, HC(6)), 10.6 (br s, 1H, HN(4)); MS (FAB) m/z $(M-H)^+$ 431.6 Calculated: 432.43.

N-(9-Fluorenylmethoxycarbonyl)-β-(cytosine-1-yl)alanine 3 [8, 9]

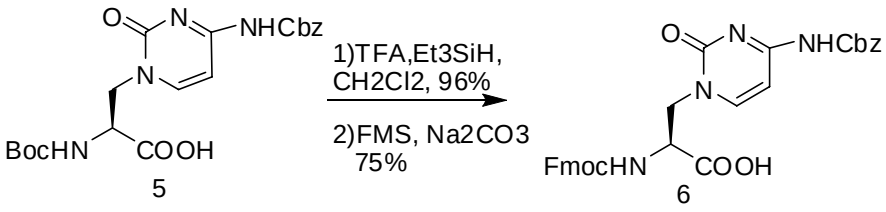

5 6

N-(tert-Butoxycarbonyl)-β-(cytosine-1-yl)alanine (**5**) (2.1 g, 4.8 mmol) was acidolysed by stirring in trifluoroacetic acid (4.8 ml, 14.4 mmol) and dichloromethane (9.8 ml, 154 mmol) in the presence of triethylsilane (1.9 ml, 12.0 mmol) at room temperature with the exclusion of moisture. After 2 hr the reaction was complete and solvent was removed. Boc-deprrotected product was readily visualized by TLC (methylene cholride/methanol (2/1) as solvent system, R_f ~0.25) by staining in ninhydrin. The residue was triturated with diethyl ether and the precipitated product (**6**) isolated by filtration (96%) ^{1}H NMR (DMSO-d_6, 400MHz) δ: 3.88 (2H, $H_2C(\beta)$), 4.29 (ddd, 1H, HC(α)), 5.16(s, 2H, $CH_2(C_6H_5)$), 6.95 (d, 1H, HC(5)), 7.32 (m, 5H, (C_6H_5)), 7.89 (d, 1H, HC(6)).

β-(cytosine-1-yl)alanine (1.4g, 4.2 mmol) was suspended in 9% sodium carbonate solution (10 ml, 8.4 mmol) and cooled in an ice bath. A solution of 9-Fluorenylmethyl N-succinimidyl carbonate (11.8 g, 3.5 mmol) in dioxan was added in one potion at 0ºC and mixing is continued at room temperature for 20 min. The mixture was diluted with water, extracted with ether and ethyl acetate. The remaining aqueous phase was cooled and acidified to pH2 with concentrated hydrochloric acid. The aqueous phase and the precipitate product was extracted with ethyl acetate, the extract was washed with saturated sodium chloride solution, water, dried with sodium sulphate, and evaporated to a small volume under reduced pressure. On addition of petroleum ether a crystalline

product **6** was obtained (75%). **6** was readily visualized by UV on TLC plate (methylene choloride/methanol (4/1) as solvent system, R_f ~0.33). ^{1}H NMR (DMSO-d_6, 400MHz) δ: 3.85/4.16 (2H, $H_2C(\beta)$), 4.22 (d, 2H), 4.37 (ddd, 1H, HC(α)), 4.4 (t, 1H), 5.15(s, 2H, $CH_2(C_6H_5)$), 6.91 (d, 1H, HC(5)), 7.28 (t, 2H), 7.32 (m, 5H, (C_6H_5)), 7.36 (t, 2H), 7.60 (d, 2H), 7.80 (d, 1H, HC(6)), 7.84 (d, 2H), 10.6 (br s, 1H, HN(4)); MS (ESI) m/z $(M+H)^+$ 555.1868 Calculated: 555.1874.

Peptide Preparation

The seven residue peptide mutant Aβ (13-21)K16AH13CyH14Cy , was synthesized with standard FMOC solid phase procedures with the N terminus free. The peptide was purified with a Water Delta 600 HPLC. Peptide product was dissolved in 3mM Tris Buffer ending with a peptide concentration of 3mM.

The seven residue peptide mutant Aβ (16-22) E22L, was synthesized with standard FMOC solid phase procedures with both N and C termini capped. The peptide monomer was dissolved in 3 mM Tris buffer/water (pH ~7) at room temperature with a final concentration of 1.3 mM. The solution became viscous immediately which indicates that the solution is mature- peptide nanotubes are present. The 1.3mM concentration was then diluted to 0.3 mM for the UV studies.

Circular Dichrosim

Samples were prepared and performed by established Circular Dichrosim procedures [11].

A quartz cuvette with a 0.1 mm path length was used with 17 μl of solution. The spectra

was scanned between 260 nm to 190 nm with a scanning rate of 100 nm/min with a resolution of 0.2 nm with a Jasco J-810 spectropolarimeter. Three wavelength scans were averaged together with the buffer control subtracted.

Titration of CyCy Peptide Nanotubes followed by Ultraviolet Visible Spectroscopy

For the UV-vis studies of CyCy peptide nanotube titrated with Adenine (Ad), Adenosine Monophosphate (AMP), or Disodium phosphate (Na_2HPO_4), solutions were prepared by the following method:

A 3 mM solution of assembled CyCy peptide nanotubes was diluted to a 0.3 mM stock solution. 0.25 mM stock solutions of Adenine, Adenosine Monophosphate, and Disodium phosphate were prepared by dissolving in 3 mM Tris buffer. 10 µl of the 0.3mM peptide nanotube stock solution was added to a 1cm path length cuvette, followed by addtion 90 µl of distilled water was added to the cuvette to have a starting volume of 100 µl. 1.6 µl of titrant (Adenine, AMP, or Na_2HPO_4) were added in 15 iterations to get a final ratio of titrant to peptide of 2:1. After each titration of 1.6 µl of the titrant a UV absorbance was taken using a Jasco UV-vis photospectrometer. The table below shows the calculations of concentrations, volumes, and ratio.

Table 3.1.1

Number	Volume of 0.3mM peptide added	Start volume	Concentration Of Titrant (mM)	Volume of Titrant added (μl)	Ending volume (μl)	Final peptide concentration (mM)	Final Titrant concentration (mM)	Titrant:Peptide concentration
1	10 μl	100 μl	0.08	1.6	101.6	0.0295	0.0039	0.13
2			0.08	1.6	103.2	0.0291	0.0078	0.27
3			0.08	1.6	104.8	0.0286	0.0115	0.40
4			0.08	1.6	106.4	0.0282	0.0150	0.53
5			0.08	1.6	108	0.0278	0.0185	0.67
6			0.08	1.6	109.6	0.0274	0.0219	0.80
7			0.08	1.6	111.2	0.0270	0.0252	0.93
8			0.08	1.6	112.8	0.0266	0.0284	1.07
9			0.08	1.6	114.4	0.0262	0.0315	1.20
10			0.08	1.6	116	0.0259	0.0345	1.33
11			0.08	1.6	117.6	0.0255	0.0374	1.47
12			0.08	1.6	119.2	0.0252	0.0403	1.60
13			0.08	1.6	120.8	0.0248	0.0430	1.73
14			0.08	1.6	122.4	0.0245	0.0458	1.87
15			0.08	1.6	124	0.0242	0.0484	2

Transmission Electron Micrograph Preparation of CyCy peptide nanotubes and Adenine, Adenosine Monophosphate, Adenosine Triphosphate.

A 10 μl aliquot of CyCy peptide solution allowed to assemble into nanotubes was applied to TEM grids (Formvar/carbon film coated 200 mesh). The solution of the CyCy peptide nanotube were allowed to absorb for 1 minute and wicked off. Uranyl acetate (5%) were placed on the TEM grid for 3 minutes and then wicked off. The TEM grid was then dried overnight under house vacuum. Preparation of the samples with CyCy peptide nanotube Ad, AMP, and Na_2HPO_4 were stained with nanotungston for 3 minutes and then wicked off. The TEM micrographs were taken on a Hitachi H -7500 transmission electron microscope instrument.

Results and Discussion

CyCy tubes would be useful as a delivery vehicle because they are: bio compatible, easy to assemble, a monolayer potentially having different inside/outside surfaces (**Figure 3.4)**. E22G tubes were unstable, more unstable then Aβ (16-22) tubes because of the glycine residue. Therefore by stabilizing the interaction between laminates like K16A+Zn^{2+} tubes, CyCy tubes should be more stable. To test if the proposed monolayer nucleobase peptide nanotubes are a good candidate as a potential delivery vehichle their stability upon dilution was investigated. Stability of the CyCy peptide nanotube was found to be stable upon dilution from 0.3 mM to 0.03 mM as shown in **Figure 3.6**. There were no ribbon structures or unraveled peptide nanotubes in the transmission electron micrographs. Although the peptide nanotubes remained intact however the peptide nanotubes in the 0.03 mM sample of peptide nanotubes diluted to 0.03 mM were noticeably shorter in length. Liu et. al have also noted that upon assembly of CyCy peptide, nanotubes were heterogeneous in length [8].

Circular dichroism of peptides can report on both conformation and peptide concentration. As shown in chapter 2, the CD signature of Aβ(16-22)E22G indicated that the peptides adopted a β-strand conformation. CyCy peptide nanotubes do not have the typical beta sheet signature that is seen in other Aβ peptide nanotubes (**Figure 2.7**) [1, 12]. The insertion of the modified cytosines could disturb the phi/psi angles of the beta sheet giving an atypical CD signature (**Figure 3.7**) for the nucleobase peptide nanotube. As a result, CD spectra can not be used to determine the secondary structure of CyCy peptide

assembled as nanotubes. More investigative CD studies need to be conducted to determine how the modified cytosines perturb the backbone to give an atypical spectra.

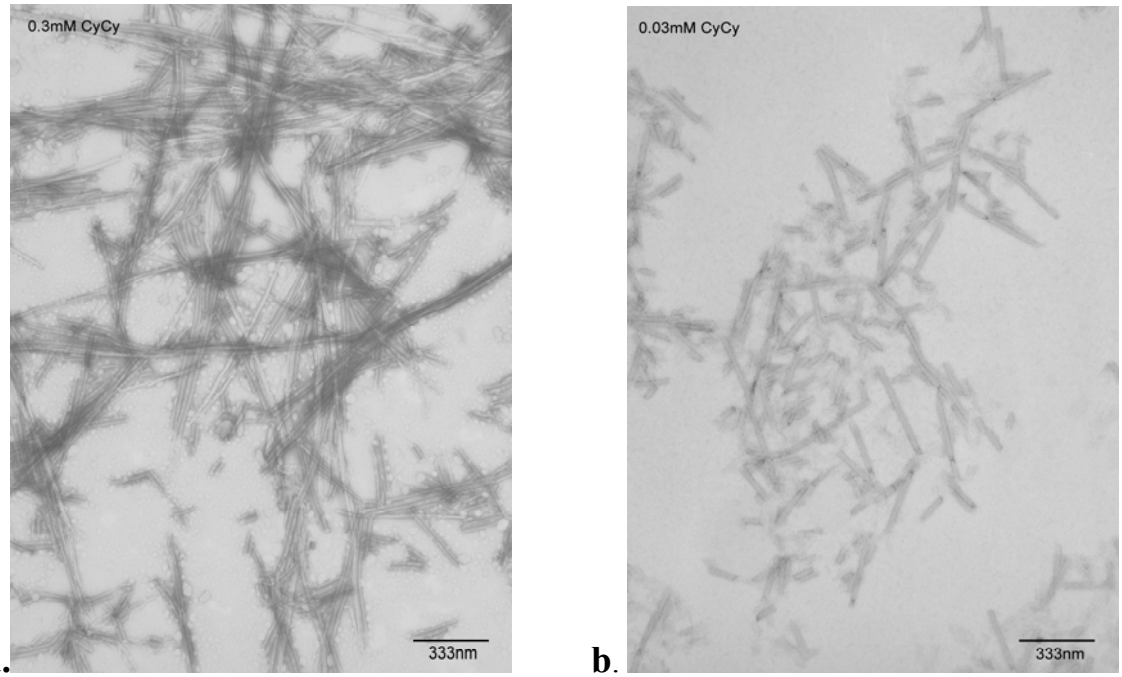

a. **b.**

Figure 3.6 a-b: a) TEM of 0.3mM CyCy peptide nanotube concentration. b) TEM after a 10-fold dilution of 0.3mM CyCy peptide nanotube solution to a 0.03mM CyCy peptide concentration.

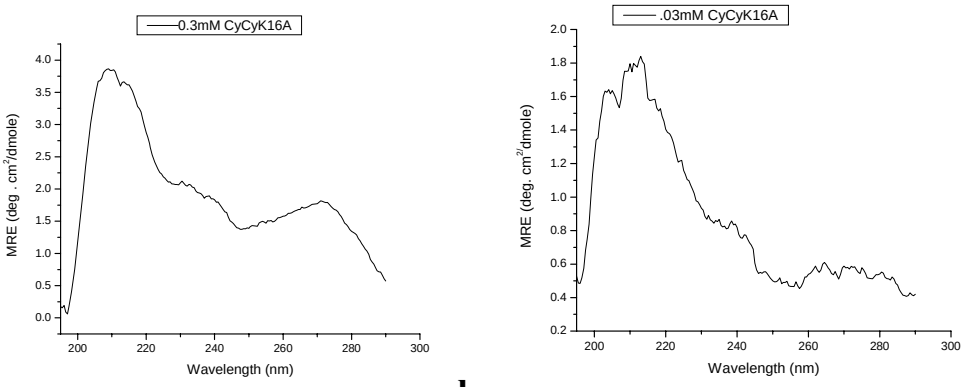

a **b**.

Figure 3.7 a-b: a) CD spectra of 0.3mM CyCy peptide nanotubes the signature has a maxima at 210nm and a minima at 255nm [8]. b) CD signature 0.03 mM CyCy peptide nanotubes.

As a result of their stability upon dilution the CyCy peptide nanotube were chosen to be used as a possible vehicle to encapsulate small molecules. In Chapter 2, I discovered that to better understand DNA interactions with peptide nanotubes it is important to see how each component affects the structure of the peptide nanotubes. As DNA consists of a nucleobase, sugar, and negatively charged backbone, the following small molecules Adenine, Adenosine Monophosphate, and Adenosine Triphosphate were chosen to investigate their interaction with CyCy peptide nanotubes. Studies with Adenine were inclusive because of the low solubility of Adenine in water.

Adenosine Monophosphate

The effects of AMP were analyzed by ultraviolet visible (UV) spectroscopy to note any absorbance changes in the spectra. UV absorbance studies show that upon titration of CyCy tubes with a chromophore (adenosine monophosphate), λ_{max} decreases and shifts. **Figure 3.8a** shows the UV spectra of AMP: CyCyQALVFFA for all ratios listed in **Table 3.1.1**. The experiment was conducted by the titration of a fixed volume of AMP to

a volume of CyCyQALVFFA. This data suggest that there may be a spectra interaction between the AMP and Cy chromophores.

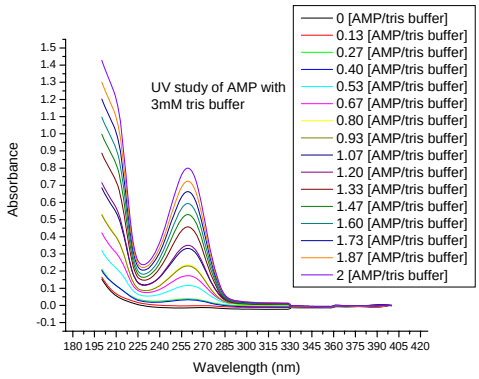

a.

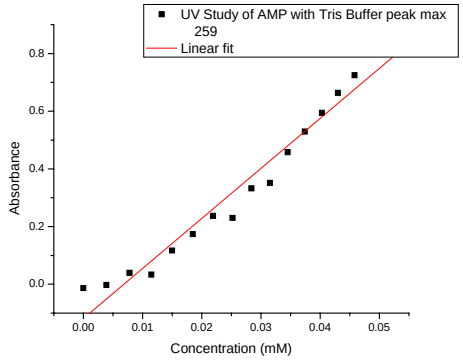

b.

Figure 3.8a-b: a) UV spectra of AMP titrated into 3 mM Tris buffer. b) Graph of λmax of AMP with Tris Buffer.

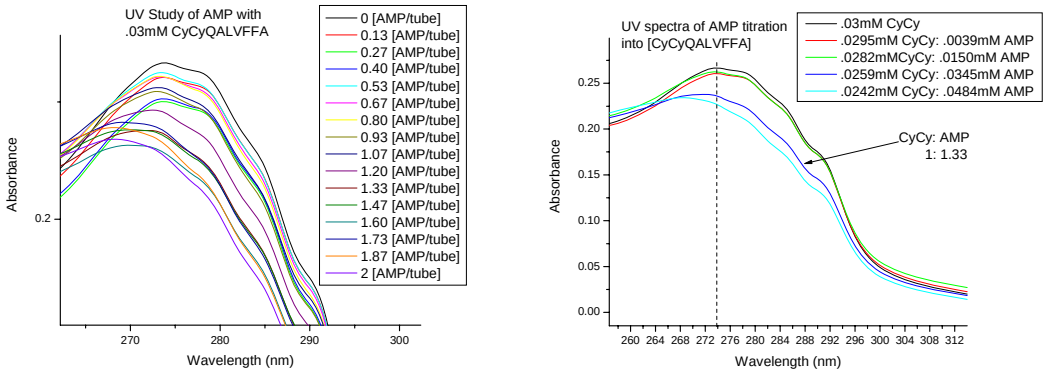

a. **b.**

Figure 3.9 a-b: a) UV spectra of AMP: CyCyQALVFFA for all ratios listed in Table 3.1.1. b) UV spectra of AMP titrated into CyCyQALVFFA assembled as nanotubes.

The observation (**Figures 3.9**) of the decrease and shift of the UV spectra of the CyCyQALVFFA and AMP is similar to the discovery that of Alexander Rich at MIT observed with his studies of polyribo A and polydeoxyribo T [13]. Rich observed upon titration of the polydeoxyribo T into a set volume of polyribo A, a decrease and shift in the UV spectra up to a 1 : 1 ratio (**Figure 3.12**) [13]. Rich's explanation in the UV spectra was due to the combination of purines and pyrmidines, which caused a decrease in the probability of the absorption (**Figure 3.10**) [13].

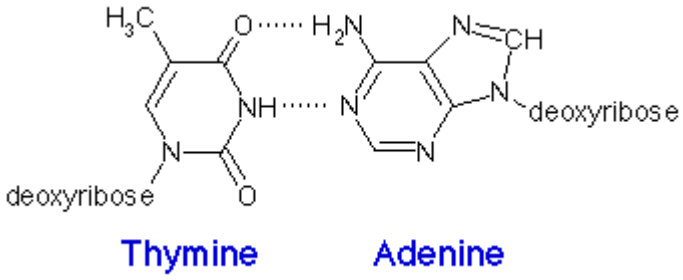

Figure 3.10: Drawing of Thymine hydrogen bonded to Adenine.

Rich further explained the observed hypochromic shift as the effect of the base pairing of the polyribo A and polydeoxyribo T [13].

In **Figure 3.11**, the black and red lines show the UV spectra for 0.0295 mM CyCy peptide nanotubes and 0.0345mM AMP respectively. The dotted blue line is the expected spectrum by summing the two CyCy and AMP UV spectra. The solid blue line is the observed spectrum of the mixture of 0.0295mM CyCy peptide nanotubes and 0.0345mM AMP. This spectrum clearly shows a decrease in the intensity of the absorbance. The nucleobase peptide nanotubes remain intact structures at the concentrations where the observed change in UV spectra is observed (.0270mM [CyCyQALVFFA] and .0252mM AMP) as shown in **Figure 3.13**. This data is consistent with AMP specifically interacting with the cytosine groups of the CyCy peptide assembled as nanotubes.

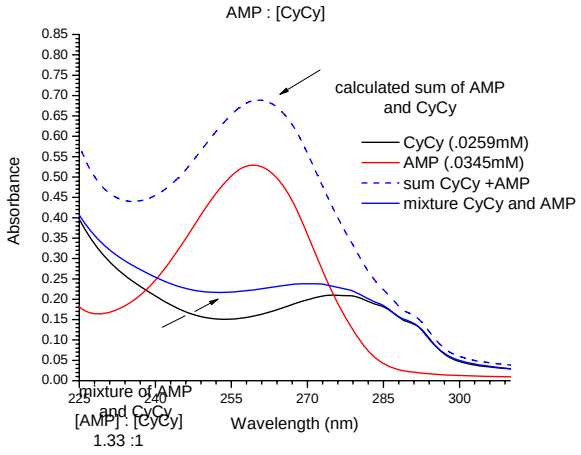

Figure 3.11. UV spectra of [AMP] : [CyCy]

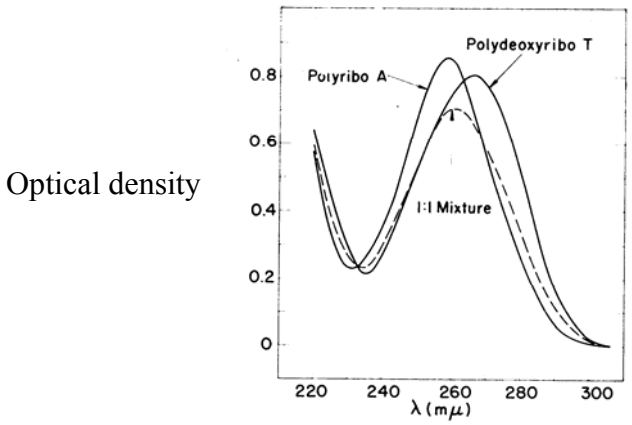

Figure 3.12: Spectra of poly A and poly T and a 1:1 mixture pH 6.9.[13]

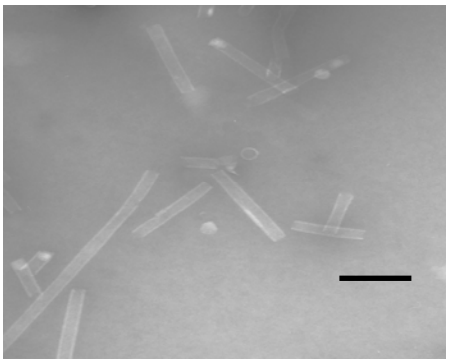

Figure 3.13: Transmission Electron Micrograph (scale 333nm) of [CyCyQALVFFA] =.0270mM [CyCyQALVFFA] to .0252mM AMP at pH 7.5, stained with nanoW.

The unique nature of this nucleobase peptide nanotube model is that the cytosines are based paired and most intercalators are used in pyrimidine/purine base pairing. The use of intercalators in DNA has shown that intercalators displace base pairs by 0.7nm from each other and the rotational angles are reduced from 36^{o} to 10^{o} [14]. Adenosine Monophosphate can be used as an intercalator, because of size and charge distribution.

Models (**Figures 3.14 and3.15**) have been developed to explain these observations. The first model examines the electrostatic interaction between the chromophore and the free N-terminus of the peptide. The negative charge from the adenosine monophosphate could result in an electrostatic attraction to the positively charge N-terminus. This association could result in the AMP and cytosine being in close proximity allowing them to interact. If this model is correct then one AMP should interact with one Aβ(13-21)K16AH13CyH14Cy peptide.

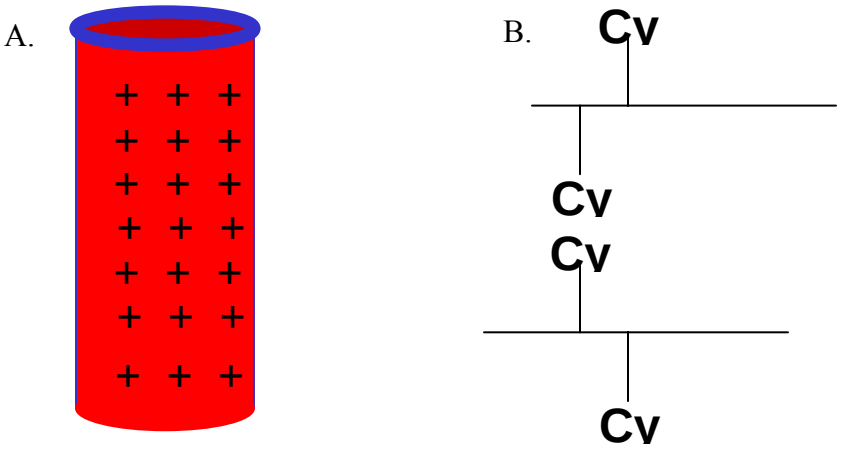

Figure 3.14 A-B: Proposed model of cytosine arrangement in nucleobase peptide nanotubes. (A) Schematic shows the charge on nanotube surface arising from the N terminus of the peptide. The distance between charges is 5Å along the long axis of the nanotube and 10Å perpendicular to the nanotube. (B) Schematic (as drawn in Figure 1 B) showing 10 Å dimension.

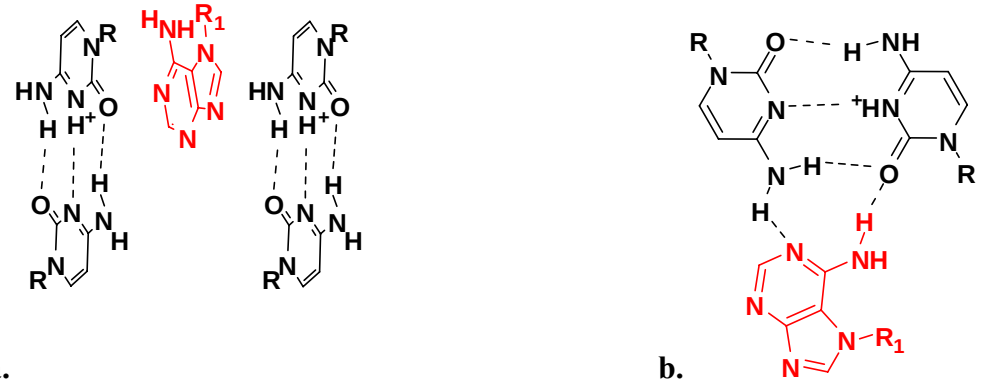

a. **b.**

Figure 3.15a-b: a) Proposed interaction of 1 AMP: 1 Cytosine. R_1 represents the ribose and monophosphate R represents the peptide backbone. b) Proposed interaction of 1 AMP : 2 Cytosines R_1 represents the ribose and monophosphate R represents the peptide backbone.

The second model is based on a binding ratio of one AMP to one peptide as shown in **Figure 3.15a**. This model is based on the possibility that one AMP π-stack per one cytosine on a peptide. The final model exploits the possibility that one AMP is hydrogen bonded to two CyCyQALVFFA as shown in **Figure 3.15b,** resulting in a peptide: AMP ratio of 2:1. Again, the electrostatic interaction between the negatively charged phosphate with the positively charged surface of the peptide nanotube could result in the two cytosines being proximial with the nucleobase of AMP. How AMP interacts with CyCy nanotubes will be investigated with ATP to investigate the effect of multiple charges.

Adenosine Triphosphate

Another curiosity was the addition of two phosphates to have three negative charges that is contributed from the chromophore. ATP was used as a chromophore in the tritration experiment to see if it necessary one charge from a chromophore to observe a hypochromic shift at the ratio of 1.33 (ATP: CyCy peptide nanotube). The UV study was performed with ATP following the calculations in **Table 3.1.1**. The findings were interesting in that at the first titration at a ratio of 0.13, ATP: peptide, the UV absorbance was 1 (Figure 3.18). Subsequently, at the ratio of 0.27, ATP: peptide, the UV absorbance was 3. Upon analysis of the TEM micrographs there were no visible structures. The overall charge of the surface of the CyCy peptide nanotube is positive which is contributed by the free N terminus that is protonated. The negative charges would cause the CyCy peptide nanotubes to aggregate however the possible interacaltion of the base leads to the disruption of the peptide nanotube.

Aβ (16-22)E22L

Studies were conducted with a peptide sequence ,Aβ (16-22)E22L, that did not include the nucleobase cytosine to investigate if there was change in the UV absorbance. 1.3mM E22L was able to form homogeneous peptide nanotubes in tris buffer/water at pH 7. **Figure 3.16** shows a CD spectrum of 1.3mM E22L in tris buffer/water at pH 7 after 13 days of incubation. A TEM micrograph of the 1.3mM E22L sample is shown.

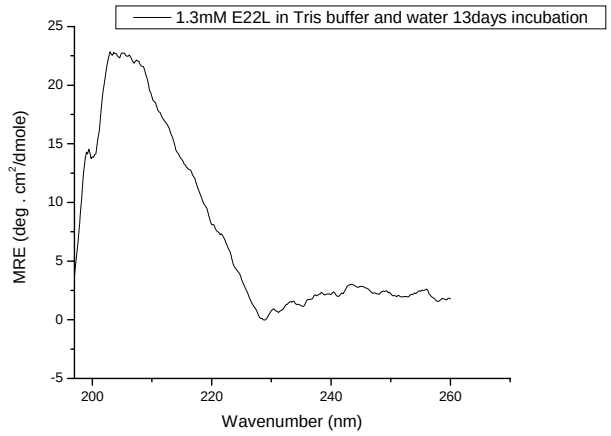

a.

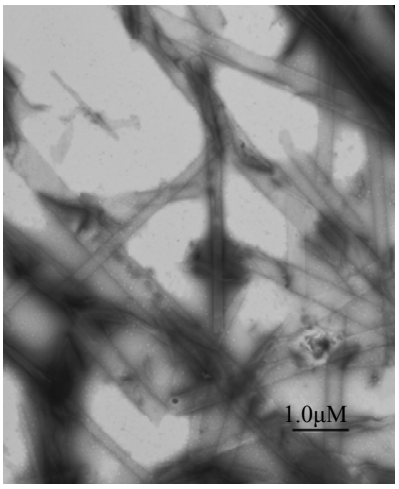

b.

Figure 3.16 a-b: a) Circular Dichorism spectrum of 1.3mM E22L in tris buffer/water at pH 7, 13 days of incubation. B) TEM micrograph of 1.3mM E22L in tris buffer/water at pH 7. The CD spectrum has the typical positive ellipicity at ~195nm and the TEM micrograph confirms the assembly of peptide nanotubes.

Conclusion

The CD spectrum has the typical positive ellipicity at ~195 nm ad the TEM micrograph confirms the assembly of peptide nanotubes. **Figure 3.17** shows the UV spectra of Aβ(16-22)E22L titrated with AMP as for the CyCy nanotubes above (**Table 3.1.1**). The UV spectrum of Aβ(16-22)E22L has a weak absorbance from 230 to 300 nm. As shown in **Figure 3.17** AMP λ_{max} is at 258nm. During the titration experiment, no hypochromic shift is observed. The UV wavelength for the peak maximum does not change for any ratio of AMP : E22L. Also the UV absorbance intensity is linearly dependent on AMP concentration. This data is consistent with no interaction between the AMP chromophore and any chromophores on Aβ(16-22)E22L. Therefore, this data is consistent with the observed hypochromic shift in CyCy peptide nanotube is contributed by the presence of the nucleobases.

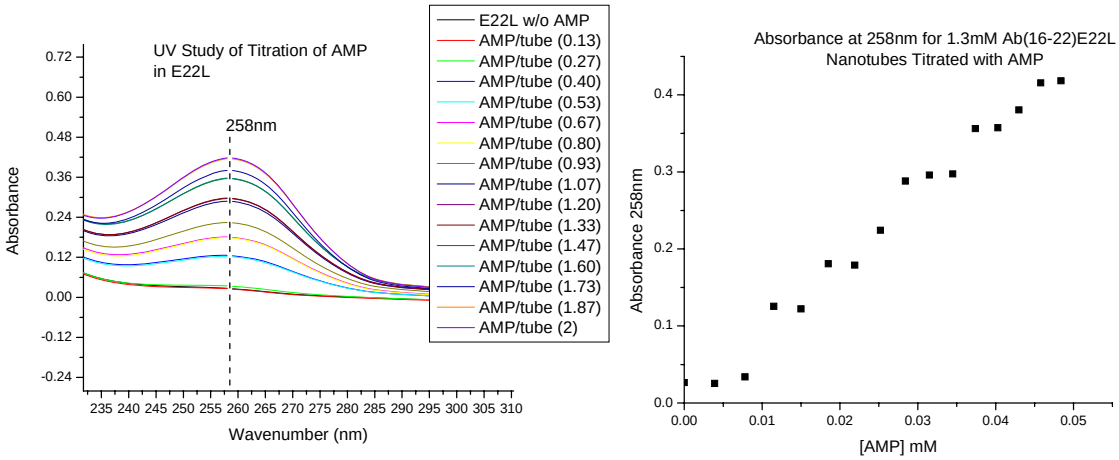

Figure 3.17 UV spectra of Aβ(16-22)E22L Titrated with AMP, λ_{max} for AMP is 258nm and indicated with a dotted line. On the right is the absorbance at 258nm plotted as a function AMP concentration.

This work has examined the use of chromophores (small molecules) and their effects on the CyCy peptide nanotube. It is evident through this study that there are potiential applications to the CyCy peptide nanotubes. It is my hope that this work can be further developed to uncover the hidden potential of the CyCy peptide nanotube and its ability to encapsulate small molecules.

Keeping with the theme of finding a peptide nanotube that could potentially encapsulate information, I have been able to use the CyCy scaffold to model a new peptide. This information gives us a platform to create new peptides with possible new properties that can help in our quest to find a delivery system that could encapsulate information.

The exciting discovery of the CyCy peptide nanotube was found by considering modifications to the Aβ(13-21)K16A peptide sequence. Liu et. al made the connection of laminate distance and nucleotide distances [2, 7]. There is a 10Å laminate distance in Aβ(13-21)K16A system [1]. Bonded bases pairs in double-helix DNA have a distance of 10-11 Å [15]. This discover led to the self-assembly of a unique system that consisted of an amyloid peptide sequence and nucleobases. Now we can think of other possible nucleobases that can be inserted into this peptide sequence to diversify the peptide sequence. Diederschen et. al. synthesis of modified nucleotides was critical in the diversification of the nucleobases in the Cy13 and Cy14 positions [9, 10].

It has been reported that the A - -T base pair (-11.8 kcal/mol) is energically less stable than the G- -C base pair (-23.8kcal/mol) [16]. The CyCy peptide nanotube is hemiprotonated at or above the pKa of the cytosine. The A- -T base pair has the potential to be protonated between laminates. It is with this question that Molecular Dyanmic (MD) simulations were performed.

Method

The Aβ(13-21)K16A sequence was modified by inserting Ad13 and Th14 in the H13 and H14 positions respectively. MD simulations with the Kollman all atom force field under NTP conditions at 300 K (coupling every 100 fs), 1 atm (coupling every 500 fs), and the compressability for the TIP waters 45.84 1e6/atm. The backbone and sidechain were held rigid and allowed to mimimize for 3 ps each. TIP water was added and allowed to equilibrate for 3 ps. The system was then opitimized at 300K.

Results and Discussion

Aβ(13-21)K16AH13AdH14Th maintaine the 10 Å between laminates.

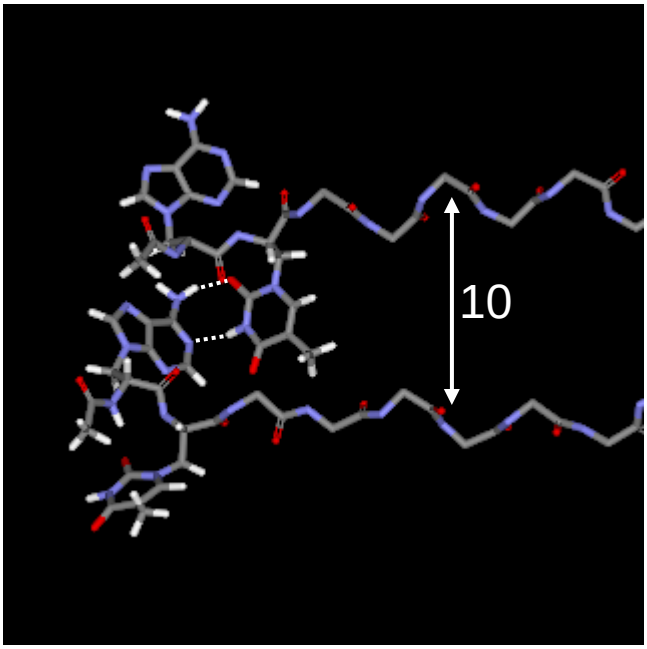

Figure 3.18 Adenine-Thymine Modified Aβ. Top view displays hydrogen bonds between Ad13 and Th14. The white dashed lines indicate hydrogen bonds.

The above MD simulation follows the pattern of previous modified Aβ systems of the stabilization of the laminate dimension that leads to the formation of peptide nanotubes. Developing novel nucleobase modified peptide nanotubes could lead to more robust peptide nanotubes and help in the understanding of the pathway to amyloid formation.

References

1. Dong, J. J.; Shokes, J. E.; Scott, R. A.; Lynn, D. G., Modulating amyloid self-assembly and fibril morphology with Zn(II). *Journal of the American Chemical Society* **2006,** 128, (11), 3540-3542.
2. Liu, P.; Lakdawala, A. S.; Lynn, D. G., Nucleobase Directed Amyloid Peptide Nanotube Formation. **In preparation**.
3. Dong, J., Shokes, Jacob, Scott, Robert, Lynn David, Modulating Amyloid Self-Assembly and Fibril Morphology win Zn (II). *Journal of the American Chemical Society* **2006,** 128, (11), 3540-3542.
4. Benzinger, T. L. S. G., D. M; Burkoth, T.S.; Miller-Aner, H; Lynn, D.G; Botto, R.E; Meredith, S.C, *Proc Natl Acad Sci U S A* **1998,** 95, 13407-13412.
5. Burkoth, T. S.; Benzinger, T. L. S.; Urban, V.; Morgan, D. M.; Gregory, D. M.; Thiyagarajan, P.; Botto, R. E.; Meredith, S. C.; Lynn, D. G., Structure of the beta-amyloid((10-35)) fibril. *Journal of the American Chemical Society* **2000,** 122, (33), 7883-7889.
6. Jijun Dong, K. L., Ami Lakdawala, Anil Mehata, David Lynn, Controlling amyloid growth i multiple dimensions. *Amyloid* **2006,** 1, (3), 206-215.
7. Lakdawala, A. S. Part I: Structure & Dynamics of beta-Amyloid Fibrils Part II: Design of Taxol (Paclitaxel) Anaologs and Predicitive Models; Design of Measles Virsu Inhibitiros; conformational Analysis of alpha-Helical Mimics. Emory University, Atlanta, 2003.
8. Liu, P. Modulating Amyloid Peptide Self-Assembly with Nucleobase Incorporation. Emory University, Atlanta, 2007.
9. Diederichsen, U., Pairing Properties of Alanyl Peptide Nucleic Acids Containing an Amino Acid Backbone wiht Alternating Configuration. *Angew. Chem. Int. Ed. Engl.* **1996,** 35, (4), 445-448.
10. Diederichsen U., W. D., Interactions of Amino Acid Side Chains with Nucleobases in Alanyl-PNA. *Synletter* **1999,** S1, 917-920.
11. Lu, K. Discovery of Diversie Peptide Nanotube Architecture form the Self-assembly of Designed Amyliod-β Cassettes. Emory University, Atlanta, 2006.
12. Lu, K.; Jacob, J.; Thiyagarajan, P.; Conticello, V. P.; Lynn, D. G., Exploiting amyloid fibril lamination for nanotube self-assembly. *J Am Chem Soc* **2003,** 125, (21), 6391-3.
13. Rich, A., A Hybrid Helix Containing Both Deoxyribose and Ribose Polynucleotides and Its Relation to the Transfer of Information between the Nucleic Acids. *Proc Natl Acad Sci U S A* **1960,** 46, (8), 1044-53.
14. Sankthakumaran, L.; Chen, A.; Pillai, C.; Thomas, T.; He, H.; Thomas, T., *Nanofabrication Towards Biomedical Applications* **2005**, 253-287.
15. Garrett, R. H. a. G., C.M., *Biochemistry*. Saunders College Publishing: Fort Worth, 1995; p 191-194.
16. Hobza, P. a. S., J., *Chem. Reve.* **1999,** 99, 3247-3276.